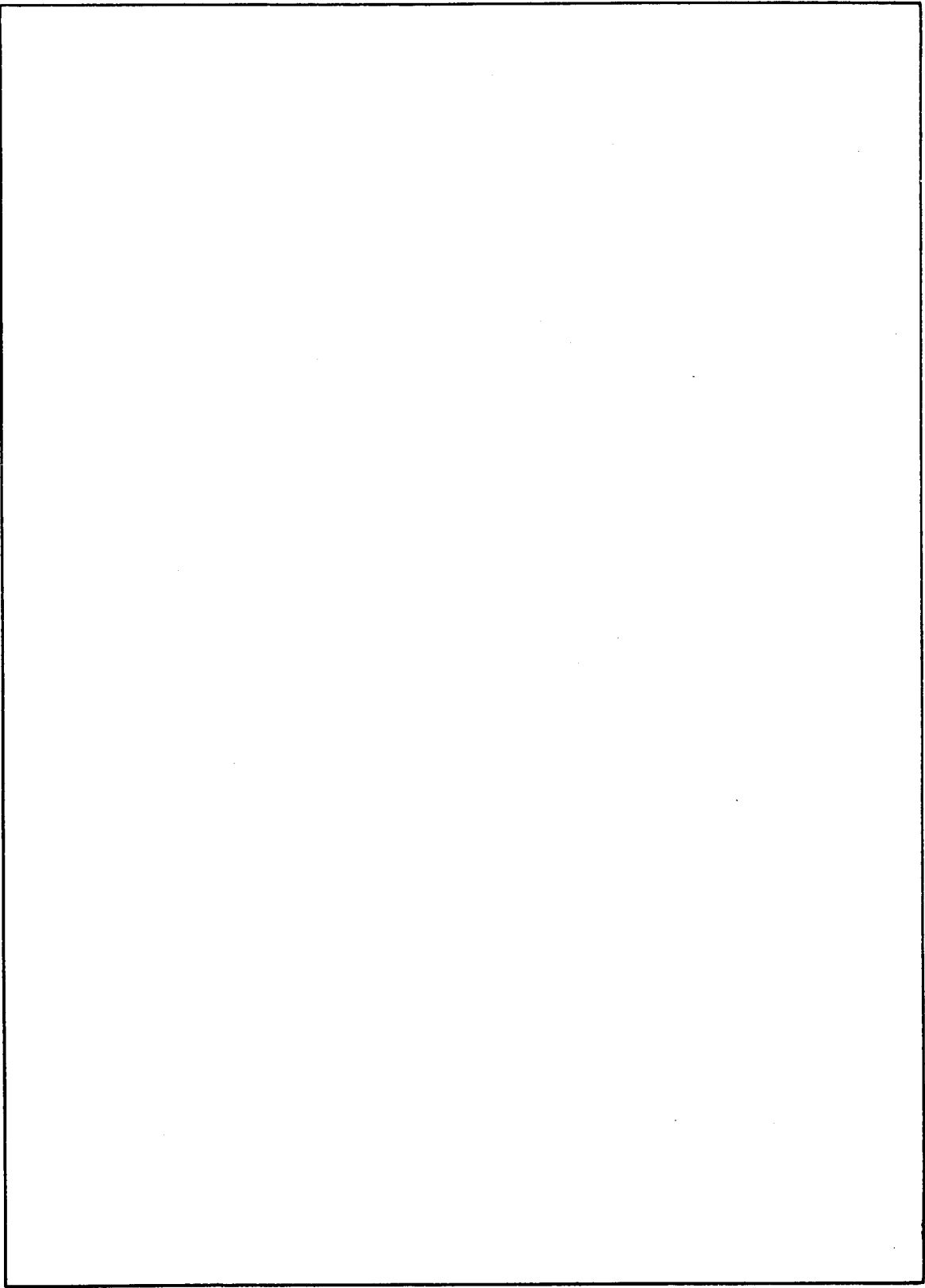


REPORT DOCUMENTATION PAGE		READ INSTRUCTIONS BEFORE COMPLETING FORM
1. REPORT NUMBER NRL Report 7868	2. GOVT ACCESSION NO.	3. RECIPIENT'S CATALOG NUMBER
4. TITLE (and Subtitle) Effect of the Lower Ionosphere on the Propagation of Waves from an ELF/VLF Source in the Magnetosphere		5. TYPE OF REPORT & PERIOD COVERED An interim report on a continuing NRL problem.
		6. PERFORMING ORG. REPORT NUMBER
7. AUTHOR(s) R. N. DeWitt Francis J. Kelly Gerald A. Chayt		8. CONTRACT OR GRANT NUMBER(s)
9. PERFORMING ORGANIZATION NAME AND ADDRESS Naval Research Laboratory Washington, D.C. 20375		10. PROGRAM ELEMENT, PROJECT, TASK AREA & WORK UNIT NUMBERS NRL Problem R07-30 Project RF 21-222-401-4360
11. CONTROLLING OFFICE NAME AND ADDRESS Department of the Navy Office of Naval Research Arlington, Virginia 22217		12. REPORT DATE April 28, 1975
		13. NUMBER OF PAGES 21
14. MONITORING AGENCY NAME & ADDRESS (if different from Controlling Office)		15. SECURITY CLASS. (of this report) UNCLASSIFIED
		15a. DECLASSIFICATION/DOWNGRADING SCHEDULE
16. DISTRIBUTION STATEMENT (of this Report) Approved for public release; distribution unlimited.		
17. DISTRIBUTION STATEMENT (of the abstract entered in Block 20, if different from Report)		
18. SUPPLEMENTARY NOTES		
19. KEY WORDS (Continue on reverse side if necessary and identify by block number) ELF/VLF waves Wave polarization Earth-ionosphere waveguide		
20. ABSTRACT (Continue on reverse side if necessary and identify by block number) A modified form of the Smith-Pitteway full-wave program is used, in conjunction with various lower ionospheric profiles, to calculate the propagation characteristics of ELF/VLF waves from a source in the magnetosphere. Expressions are developed which give the ratio of the power transmitted into the earth's surface to the power incident on the ionosphere as a function of the number of wave hops in the earth-ionosphere waveguide. The wave polarization after each hop is obtained showing a limiting polarization after several hops. Numerical evaluation of these expressions are presented and discussed.		



CONTENTS

INTRODUCTION	1
THEORY	2
CALCULATION AND RESULTS	8
Ionospheric Profiles	8
Reflection Coefficients	8
Calculation of the Transmission Coefficient.	8
CONCLUSION	16
REFERENCES	17

EFFECT OF THE LOWER IONOSPHERE ON THE PROPAGATION OF WAVES FROM AN ELF/VLF SOURCE IN THE MAGNETOSPHERE

INTRODUCTION

In considering undersea reception from a source radiating extremely-low-frequency (ELF) or very-low-frequency (VLF) waves in the magnetosphere, it is necessary to calculate a factor which takes into account the attenuation of the waves caused by their transmission through the ionosphere, the possible multiple reflection in the earth-ionosphere waveguide, and the penetration of the sea surface. This factor is defined as the ratio of the plane-wave power per unit area at the submerged receiver antenna to the plane-wave power per unit area incident on top of the lower ionosphere. We will refer to this factor as a TRP factor in this report since its evaluation depends, in general, on a knowledge of the ionospheric transmission (T), reflection (R), and resultant polarization (P) of the waves. In producing a complete signal-level prediction from a given source, additional important factors must be evaluated, such as the radiated power pattern of the antenna and the spreading factor of the waves. These terms and their combination to provide a total power budget will be treated in subsequent reports. The objective of this report is to describe a technique for evaluating the TRP factor and to present examples of calculated results.

For long wavelengths the lower region of the ionosphere experiences substantial gradients in electron concentration. These gradients give rise to internal reflections, mode coupling, and collisional absorption. Therefore a full-wave method of calculation is necessary within the ionosphere, as opposed to a ray method or W.K.B. method.

Pitteway [1, 2] has studied the transmission, reflection, and polarization characteristics of long-wavelength radio waves propagating through the ionosphere using a full-wave computer method. By integrating the governing differential equations downward through the ionosphere, two characteristic solutions (the penetrating and nonpenetrating modes) are generated. The penetrating-mode solution is defined by choosing the polarization of the modes where the wave is incident on the ionosphere from below, in such a way as to maximize the energy transmitted to the whistler-mode wave at great heights. By properly comparing the two solutions, reflection and transmission coefficients can be obtained as a function of polarization. The method has been successful in overcoming limitations and numerical instabilities of previous methods. Scarabucci [3] has done some work in extending this method to include the effects of heavy ions.

Pappert et al. [4-6] have developed a program for numerically determining mode conversion coefficients and mode sums for propagation in an earth-ionosphere waveguide. Using this program, vertical and horizontal electric-field mode sums are calculated for

Note: Manuscript submitted January 24, 1975.

vertical, horizontal, and inclined point-dipole radiators. Reflection coefficients for the ionosphere and ground are treated in the manner developed by Budden [7] and Wait et al. [8]. Their method for calculating ionospheric reflection coefficients is similar to that used by Pitteway in that the governing equations of the ionospheric reflection coefficient are integrated downward in a step-by-step process. However, their method cannot determine wave fields inside the ionosphere and hence the power transmitted from sources high in the ionosphere.

In the next section we derive the theory behind the TRP factor, which displays its dependence on quantities obtainable from Pitteway's program in treating the propagation of waves through the ionosphere. These results include a novel method for determining the wave polarization as a function of the number of hops in the earth-ionosphere waveguide. This is accomplished by introducing a new set of basis vectors for the E field obtained through the diagonalization of the reflection matrix for a single hop. It is seen that, in general, a limiting polarization is attained after several hops. In the third section we describe some calculations and results, for specific ionospheric models, obtained by using Pitteway's technique, combined with the use of the TRP factor.

THEORY

Consider a signal being transmitted from a satellite into the sea. Let the wave be incident on the upper boundary of the ionosphere at an angle ϑ_i (Fig. 1), exit the ionosphere at an angle ϑ_a , and then refract into the sea. Since the wave entering the sea will, in general, be elliptically polarized, the field components of the wave can be resolved into components E_{\parallel} , H_{\parallel} parallel to the plane of incidence and E_{\perp} , H_{\perp} perpendicular to that plane. Using the notation of Kraichman [9], the Poynting vector for the E_{\parallel} case (TM mode) is, with the asterisk denoting the complex conjugate,

$$\mathbf{\Pi} = \frac{1}{2} \text{Re} (\mathbf{E} \times \mathbf{H}^*) = \frac{1}{2} \text{Re} \left[\frac{-i\omega}{\gamma} (\hat{k} \times \mathbf{H}) \times \mathbf{H}^* \right] = \frac{\omega}{2} |\mathbf{H}|^2 \frac{\text{Im}(\gamma)}{|\gamma|^2} \hat{k}, \quad (1)$$

where $\gamma^2 = -\omega^2 \epsilon + i\omega \sigma$ and \hat{k} is a unit vector in the direction of propagation. Defining a transmission coefficient T_{\parallel} as the ratio of the normal component of the Poynting vector in the sea ($\Pi_{s,z}$) to the normal component in air ($\Pi_{a,z}$) and realizing that the energy flow in a good conductor (for example the sea) is perpendicular to the surface, there results for the E_{\parallel} case (TM mode)

$$T_{\parallel} = \frac{\Pi_{s,z}^{(\parallel)}}{\Pi_{a,z}^{(\parallel)}} = \frac{\text{Im}(\gamma_s) |\gamma_a|^2 \left| \frac{H_s}{H_a} \right|^2}{\text{Im}(\gamma_a) |\gamma_s|^2 \cos \vartheta_a} = \frac{\text{Im}(\gamma_s) |\gamma_a|^2 |\tau_{TM}|^2}{\text{Im}(\gamma_a) |\gamma_s|^2 \cos \vartheta_a}, \quad (2)$$

where

$$\tau_{TM} = \frac{2\gamma_s^2 \cos \vartheta_a}{\gamma_s^2 \cos \vartheta_a + \gamma_a \sqrt{\gamma_s^2 - \gamma_a^2 \sin^2 \vartheta_a}}. \quad (3)$$

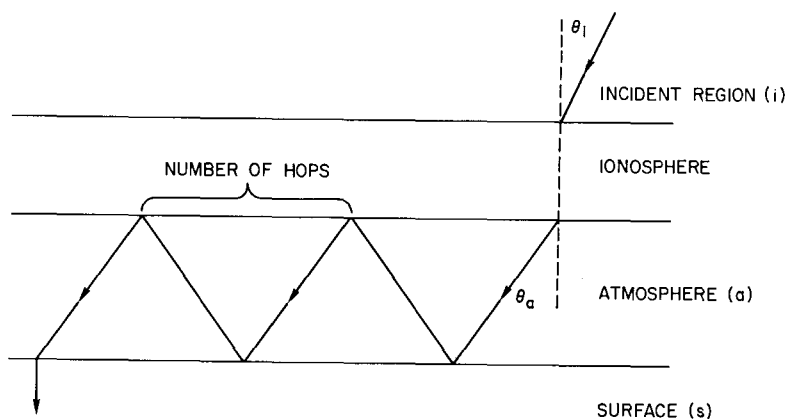


Fig. 1 — Notation for a wave incident on the ionosphere at an angle ϑ_i , exiting at an angle ϑ_a , and penetrating the sea

Likewise the Poynting vector for the E_1 case (TE mode) is

$$\mathbf{\Pi} = \frac{1}{2} \text{Re} \left[\frac{\gamma}{i\omega} \mathbf{E} \times (\hat{k} \times \mathbf{E}^*) \right] = \frac{|E|^2}{2\omega} \text{Im}(\gamma) \hat{k}, \quad (4)$$

giving

$$T_{\perp} = \frac{\Pi_{s,z}^{(\perp)}}{\Pi_{a,z}^{(\perp)}} = \frac{\text{Im}(\gamma_s) |\tau_{TE}|^2}{\text{Im}(\gamma_a) \cos \vartheta_a}, \quad (5)$$

where

$$\tau_{TE} = \frac{2\gamma_a \cos \vartheta_a}{\gamma_a \cos \vartheta_a + \sqrt{\gamma_s^2 - \gamma_a^2} \sin^2 \vartheta_a} \quad (6)$$

Therefore the normal component of the total Poynting vector in the sea is given by

$$\Pi_{s,z} = T_{\perp} \Pi_{a,z}^{(\perp)} + T_{\parallel} \Pi_{a,z}^{(\parallel)}. \quad (7)$$

Using the notation of Pitteway [1], the ratio of the two components $\Pi^{(\perp)}$ and $\Pi^{(\parallel)}$ of a wave related through

$$\frac{\Pi^{(\perp)}}{\Pi^{(\parallel)}} = \left| \frac{E_{\perp}}{E_{\parallel}} \right|^2 = |a|^2 \quad (8)$$

gives for the normal components of the Poynting vector in the atmosphere

$$\Pi_{a,z}^{(\parallel)} = \frac{\Pi_{a,z}^{(\text{total})}}{1 + |a|^2}; \quad \Pi_{a,z}^{(\perp)} = \frac{|a|^2 \Pi_{a,z}^{(\text{total})}}{1 + |a|^2}. \quad (9)$$

Pitteway also defines a transmission coefficient T^2 for the ionosphere as

$$T^2 = \frac{\Pi_{a,z}^{(total)}}{\Pi_{i,z}^{(total)}} , \quad (10)$$

where $\Pi_{i,z}^{(total)}$ is the normal component of the total Poynting vector incident on top of the ionosphere.

Thus Eq. (7) can be written as

$$\Pi_{s,z} = \frac{T^2 \Pi_{i,z}^{(total)}}{1 + |a|^2} \left[T_{\perp} |a|^2 + T_{\parallel} \right]. \quad (11)$$

From Eqs. (2) and (5) the ratio of T_{\parallel} to T_{\perp} is

$$\frac{T_{\parallel}}{T_{\perp}} = \frac{|\gamma_a|^2 |\tau_{TM}|^2}{|\gamma_s|^2 |\tau_{TE}|^2} ,$$

which, after using Eqs. (3) and (6), gives

$$\frac{T_{\parallel}}{T_{\perp}} = \left| \frac{\gamma_s (\gamma_a \cos \vartheta_a + \sqrt{\gamma_s^2 - \gamma_a^2 \sin^2 \vartheta_a})}{\gamma_s^2 \cos \vartheta_a + \gamma_a \sqrt{\gamma_s^2 - \gamma_a^2 \sin^2 \vartheta_a}} \right|^2 \quad (12)$$

In comparing electrical characteristics of the sea and the atmosphere, it is found that $\gamma_s \gg \gamma_a$, and Eq. (12) can be written as

$$T_{\perp} \approx T_{\parallel} \cos^2 \vartheta_a . \quad (13)$$

This allows Eq. (11) to be written as

$$\Pi_{s,z} = T^2 \Pi_{i,z}^{(total)} \frac{T_{\parallel}}{1 + |a|^2} (1 + |a|^2 \cos^2 \vartheta_a) . \quad (14)$$

Equation (2) can be rewritten as

$$T_{\parallel} = \frac{T_g}{\cos \vartheta_a} ,$$

where

$$T_g = \frac{Im(\gamma_s) |\gamma_a|^2}{Im(\gamma_a) |\gamma_s|^2} \left| \frac{2\gamma_s^2 \cos \vartheta_a}{\gamma_s^2 \cos \vartheta_a + \gamma_a \sqrt{\gamma_s^2 - \gamma_a^2 \sin^2 \vartheta_a}} \right|^2 . \quad (15)$$

With $\gamma_s \gg \gamma_a$ and ϑ_a not too far from the vertical, T_g will be nearly constant. Therefore, Eq. (14) can be written as

$$\frac{\Pi_{s,z}}{\Pi_{i,z}^{(\text{total})}} = \frac{T^2 T_g (1 + |a|^2 \cos^2 \vartheta_a)}{(1 + |a|^2) \cos \vartheta_a}. \quad (16)$$

If the signal reflects once from the earth and then from the lower boundary of the ionosphere, the fields are related by

$$\begin{pmatrix} E_{\parallel} \\ E_{\perp} \end{pmatrix}^{(1)} = \begin{pmatrix} R_{\parallel} & R_{\perp} \\ R_{\perp} & R_{\parallel} \end{pmatrix} \begin{pmatrix} 1 & 0 \\ 0 & -1 \end{pmatrix} \begin{pmatrix} E_{\parallel} \\ E_{\perp} \end{pmatrix}^{(0)} = \begin{pmatrix} R_{\parallel} - R_{\perp} \\ R_{\perp} - R_{\parallel} \end{pmatrix} \begin{pmatrix} E_{\parallel} \\ E_{\perp} \end{pmatrix}^{(0)}, \quad (17)$$

where the components of the reflection matrix have their standard meaning (Ref. 7). By induction, after N reflections from the earth and then the ionosphere the fields are related by

$$\begin{pmatrix} E_{\parallel} \\ E_{\perp} \end{pmatrix}^{(N)} = \mathbf{R}^{(N)} \begin{pmatrix} E_{\parallel} \\ E_{\perp} \end{pmatrix}^{(0)} \quad (18)$$

where

$$\mathbf{R}^{(N)} = \begin{pmatrix} R_{11}^{(N)} & R_{12}^{(N)} \\ R_{21}^{(N)} & R_{22}^{(N)} \end{pmatrix} = \begin{pmatrix} R_{\parallel} & -R_{\perp} \\ R_{\perp} & -R_{\parallel} \end{pmatrix}^N \quad (19)$$

The normal component of the total Poynting vector in the sea will now be given by

$$\Pi_{s,z}^{(N)} = T_{\perp} \Pi_{a,z}^{(\perp)(N)} + T_{\parallel} \Pi_{a,z}^{(\parallel)(N)}. \quad (20)$$

Using Eqs. (18) and (19) and the relations

$$\Pi_a^{(\perp)(N)} \propto |E_{\perp,a}^{(N)}|^2, \quad \Pi_a^{(\parallel)(N)} \propto |E_{\parallel,a}^{(N)}|^2, \quad \Pi_{a,z}^{(\parallel)} = \frac{\Pi_{a,z}^{(\text{total})}}{1 + |a|^2}, \quad (21)$$

Eq. (20) becomes

$$\Pi_{s,z}^{(N)} = \frac{\Pi_{a,z}^{(\text{total})}}{1 + |a|^2} \left[T_{\parallel} |R_{11}^{(N)} + R_{12}^{(N)} a|^2 + T_{\perp} |R_{21}^{(N)} + R_{22}^{(N)} a|^2 \right]. \quad (22)$$

Using the same approximations leading to Eq. (16) allows Eq. (22) to be written as

$$\frac{\Pi_{s,z}^{(N)}}{\Pi_{i,z}^{(\text{total})}} = \frac{|T|^2 T_g}{(1 + |a|^2) \cos \vartheta_a} \left[|R_{11}^{(N)} + R_{12}^{(N)} a|^2 + \cos^2 \vartheta_a |R_{21}^{(N)} + R_{22}^{(N)} a|^2 \right]. \quad (23)$$

The right side of this equation is called the TRP factor. When $N = 0$, \mathbf{R} is a unit matrix, and Eq. (23) reduces to Eq. (16). Thus the TRP factor for multiple hops between the ground and ionosphere reduces to the zero-hop TRP factor.

Since the components of $R^{(N)}$ are obtained by raising a matrix to the N th power, much mixing of parallel and perpendicular wave components results. In addition, each component of the matrix is a complex number, causing the sense of polarization to change after each reflection. If the polarization is characterized by the complex polarization amplitude a , the change in polarization after each hop is determined by the equation

$$a^{(N)} = \frac{R_{21}^{(1)} + R_{22}^{(1)} a^{(N-1)}}{R_{11}^{(1)} + R_{12}^{(1)} a^{(N-1)}}, \quad (24)$$

where each quantity is a complex number. In fact, if the complex numbers are represented by

$$a^{(N-1)} = \alpha + i\beta, \quad (25a)$$

$$R_{ij}^{(1)} = \alpha_{ij} + i\beta_{ij}, \quad (25b)$$

the real part of the polarization amplitude after N hops is given by

$$Re[a^{(N)}] = \frac{(\alpha_{21} + \alpha_{22}\alpha - \beta_{22}\beta)(\alpha_{11} + \alpha_{12}\alpha - \beta_{12}\beta) + (\beta_{21} + \beta_{22}\alpha + \alpha_{22}\beta)(\beta_{11} + \beta_{12}\alpha + \alpha_{12}\beta)}{(\alpha_{11} + \alpha_{12}\alpha - \beta_{12}\beta)^2 + (\beta_{11} + \beta_{12}\alpha + \alpha_{12}\beta)^2} \quad (26a)$$

and the imaginary part by

$$Im[a^{(N)}] = \frac{(\alpha_{11} + \alpha_{12}\alpha - \beta_{12}\beta)(\beta_{21} + \beta_{22}\alpha + \alpha_{22}\beta) - (\alpha_{21} + \alpha_{22}\alpha - \beta_{22}\beta)(\beta_{11} + \beta_{12}\alpha + \alpha_{12}\beta)}{(\alpha_{11} + \alpha_{12}\alpha - \beta_{12}\beta)^2 + (\beta_{11} + \beta_{12}\alpha + \alpha_{12}\beta)^2} \quad (26b)$$

Thus it is explicitly seen that the sense of polarization after each hop is determined by the relative magnitudes of the components given in Eq. (25). However, if the number of hops is large, it is difficult to determine the sense of polarization. This can be overcome in the following way.

Recall Eqs. (18) and (19):

$$\begin{pmatrix} E_{\parallel} \\ E_{\perp} \end{pmatrix}^{(N)} = \mathbf{R}^{(N)} \begin{pmatrix} E_{\parallel} \\ E_{\perp} \end{pmatrix}^{(0)} \quad (18)$$

$$\mathbf{R}^{(N)} = \begin{pmatrix} \parallel R_{\parallel} & -\perp R_{\parallel} \\ \parallel R_{\perp} & -\perp R_{\perp} \end{pmatrix}^N \quad (19)$$

From the eigenvalue equation

$$\begin{pmatrix} \|R_{\parallel} - \lambda & -_{\perp}R_{\parallel} \\ \|R_{\perp} & -_{\perp}R_{\perp} - \lambda \end{pmatrix} \begin{pmatrix} U_1 \\ U_2 \end{pmatrix} = 0, \quad (27)$$

a matrix \mathbf{Q} can be constructed which will diagonalize $\mathbf{R}^{(1)}$. That is, for Eq. (27) to have solutions, the following must be satisfied:

$$\begin{vmatrix} \|R_{\parallel} - \lambda & -_{\perp}R_{\parallel} \\ \|R_{\perp} & -_{\perp}R_{\perp} - \lambda \end{vmatrix} = 0.$$

Thus λ satisfies a quadratic equation with the two solutions

$$\lambda = \frac{1}{2} (\|R_{\parallel} -_{\perp}R_{\perp}) \pm \frac{1}{2} \sqrt{(\|R_{\parallel} -_{\perp}R_{\perp})^2 - 4(\|R_{\perp} _{\perp}R_{\parallel} - \|R_{\parallel} _{\perp}R_{\perp})}.$$

Denoting the solution with the positive sign by λ_p and that with the negative sign by λ_n , the matrix \mathbf{Q} will then be

$$\mathbf{Q} = \begin{pmatrix} \frac{1}{U_p} & \frac{1}{U_n} \\ \frac{\|R_{\parallel} - \lambda_p}{_{\perp}R_{\parallel} U_p} & \frac{\|R_{\parallel} - \lambda_n}{_{\perp}R_{\parallel} U_n} \end{pmatrix},$$

where

$$U_p^2 = 1 + \left| \frac{\|R_{\parallel} - \lambda_p}{_{\perp}R_{\parallel}} \right|^2, \quad U_n^2 = 1 + \left| \frac{\|R_{\parallel} - \lambda_n}{_{\perp}R_{\parallel}} \right|^2.$$

Multiplying Eq. (18) on the left by \mathbf{Q}^{-1} and using $\mathbf{Q}\mathbf{Q}^{-1} = \mathbf{1}$ gives

$$\mathbf{Q}^{-1} \mathbf{E}^{(N)} = (\mathbf{Q}^{-1} \mathbf{R}^{(1)} \mathbf{Q})^N \mathbf{Q}^{-1} \mathbf{E}^{(0)}. \quad (28)$$

But since \mathbf{Q} diagonalizes $\mathbf{R}^{(1)}$, there results

$$\begin{pmatrix} Q_{11}^{-1} & Q_{12}^{-1} \\ Q_{21}^{-1} & Q_{22}^{-1} \end{pmatrix} \begin{pmatrix} E_{\parallel}^{(N)} \\ E_{\perp}^{(N)} \end{pmatrix} = \begin{pmatrix} \lambda_p^N & 0 \\ 0 & \lambda_n^N \end{pmatrix} \begin{pmatrix} Q_{11}^{-1} & Q_{12}^{-1} \\ Q_{21}^{-1} & Q_{22}^{-1} \end{pmatrix} \begin{pmatrix} E_{\parallel}^{(0)} \\ E_{\perp}^{(0)} \end{pmatrix}, \quad (29)$$

where Q_{ij}^{-1} denotes the components of \mathbf{Q}^{-1} . Taking ratios of the vector components and using the definitions

$$a(0) = \frac{E_{\perp}(0)}{E_{\parallel}(0)}, \quad a(N) = \frac{E_{\perp}(N)}{E_{\parallel}(N)} \quad (30)$$

gives

$$a^{(N)} = \frac{Q_{21}^{-1} \left[\left(\frac{\lambda_p}{\lambda_n} \right)^N \frac{Q_{11}^{-1} + Q_{12}^{-1} a^{(0)}}{Q_{21}^{-1} + Q_{22}^{-1} a^{(0)}} \right] - Q_{11}^{-1}}{Q_{12}^{-1} - Q_{22}^{-1} \left[\left(\frac{\lambda_p}{\lambda_n} \right)^N \frac{Q_{11}^{-1} + Q_{12}^{-1} a^{(0)}}{Q_{21}^{-1} + Q_{22}^{-1} a^{(0)}} \right]}. \quad (31)$$

This is an explicit expression for the polarization parameter after N hops. Equation (31) now shows that there will be two limiting cases for the polarization parameter when N is large, namely

$$a^{(N)} \rightarrow - \frac{Q_{11}^{-1}}{Q_{12}^{-1}} \quad \text{when} \quad \left| \frac{\lambda_p}{\lambda_n} \right| < 1; \quad (32a)$$

$$a^{(N)} \rightarrow - \frac{Q_{21}^{-1}}{Q_{22}^{-1}} \quad \text{when} \quad \left| \frac{\lambda_p}{\lambda_n} \right| > 1. \quad (32b)$$

Note that each limit is independent of the initial polarization, unless $|\lambda_p/\lambda_n| = 1$.

CALCULATIONS AND RESULTS

Ionospheric Profiles

To make calculations of ionospheric reflection and transmission coefficients, ionospheric electron-density and collision-frequency profiles are required. For our present calculations we have used a daytime profile of the lower ionospheric electron density and collision frequency [10] and a nighttime profile [11].

Reflection Coefficients

We used the computer programs of Pappert et al. [12] and Smith and Pitteway [13] to calculate reflection coefficients $|_{\parallel}R_{\parallel}|$, $|_{\perp}R_{\perp}|$, $|_{\parallel}R_{\perp}|$, and $|_{\perp}R_{\parallel}|$ and obtained good agreement for these quantities using the two different programs (Table 1). Figures 2 through 4 show values of the reflection coefficients as a function of angle of incidence on the ionosphere for the nighttime ionospheric profile.

Calculation of the Transmission Coefficient

The Smith-Pitteway full-wave program was used, in conjunction with the Galejs nighttime ionospheric profile, to calculate whistler-mode transmission and reflection coefficients, given a frequency of 3 kHz, a dip angle of 60° , and various values of the

Table 1
 Comparison of the Results of the Pappert Program and the
 Pitteway Program for a Daytime ($\beta = 0.5 \text{ km}^{-1}$, $h = 70 \text{ km}$)
 ionosphere at 2 kHz

θ (degrees)	$\parallel R_{\parallel}$		$\perp R_{\perp}$	
	Pappert	Pitteway	Pappert	Pitteway
0	0.7738	0.76286	0.7738	0.76286
30	0.7109	0.696809	0.8009	0.79198
45	0.6314	0.6163	0.8340	0.8259
60	0.5288	0.5215	0.8798	0.8735

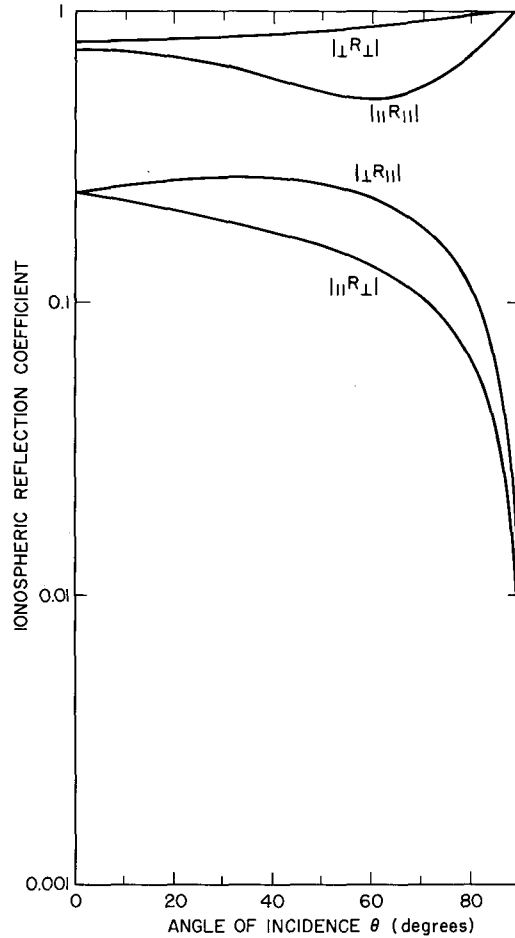


Fig. 2 — Nighttime ionospheric reflection coefficients
 for 3 kHz east-to-west propagation

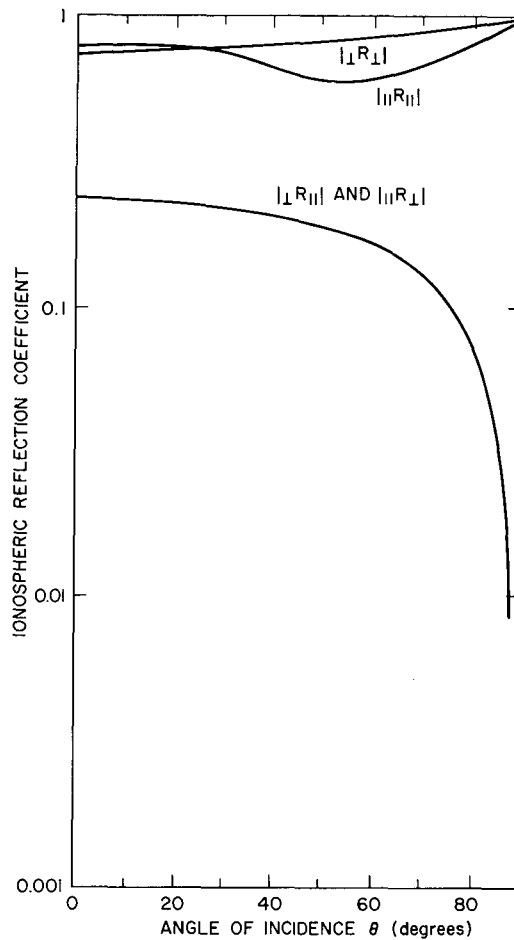


Fig. 3 — Nighttime ionospheric reflection coefficients for 3 kHz south-to-north propagation

angle of incidence and azimuth, measured from magnetic north. The top and bottom heights were set equal to 120 km and 67.5 km respectively. Figures 5 and 6, along with Tables 2 through 4, show the results of these calculations.

It was first established that a step size of one hundredth of a wavelength ($\lambda/100$) was suitable for the calculations. In Table 3, for instance, comparison of lines 2 and 3, or lines 5 and 6, or lines 8 and 9, reveals considerable differences in the transmission coefficients when a step size of $\lambda/50$ is used instead of $\lambda/100$. On the other hand, comparison of lines 1 and 2 of Table 4 reveals that the transmission coefficient remains constant to three significant figures when the step size is increased from $\lambda/1000$ to $\lambda/100$.

Figure 5, obtained from Table 2, shows the variation of the transmission and reflection coefficients with the angle of incidence PHI for a fixed azimuth $AZ = 0^\circ$. The transmission coefficient varies from a minimum value at large magnitude of PHI to a maximum

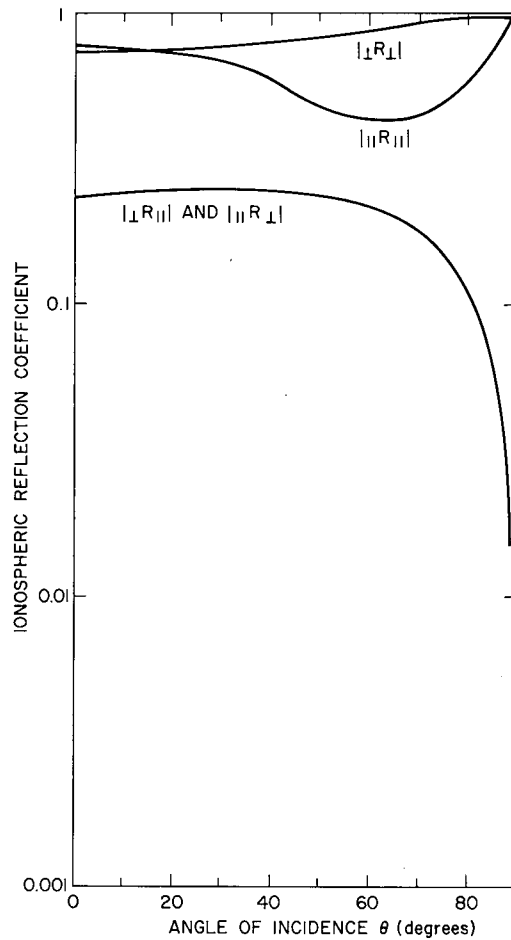


Fig. 4 — Nighttime ionospheric reflection coefficients for 3 kHz west-to-east propagation

value within a region of PHI near 0° . Furthermore, the transmission coefficient is not completely symmetrical about $PHI = 0^\circ$. The reflection coefficient varies from a maximum value at large values of PHI to a minimum value near $PHI = 0^\circ$, although the variation is only slight (from about 0.606 at $PHI = -85^\circ$ to 0.527 at $PHI = 0^\circ$) and is more symmetrical than the transmission coefficient.

Figure 6, obtained from Tables 2 and 4, shows a family of graphs of transmission coefficients and reflection coefficients as a function of azimuth for fixed values of PHI equal to 30° , 60° , and 85° . Since computations are made for few values of AZ , adjacent points of the same graph are joined by a straight line. For a fixed value of PHI , the transmission coefficients seem to decrease as the azimuth increases from 0° , but they increase as the azimuth approaches 270° . The transmission coefficient for any fixed azimuth decreases as PHI increases from 30° to 85° . The reflection coefficients seem to increase slightly as the azimuth increases from 0° , but they decrease as the azimuth approaches 270° . The reflection coefficient for any fixed azimuth increases slightly as PHI increases from 30° to 85° .

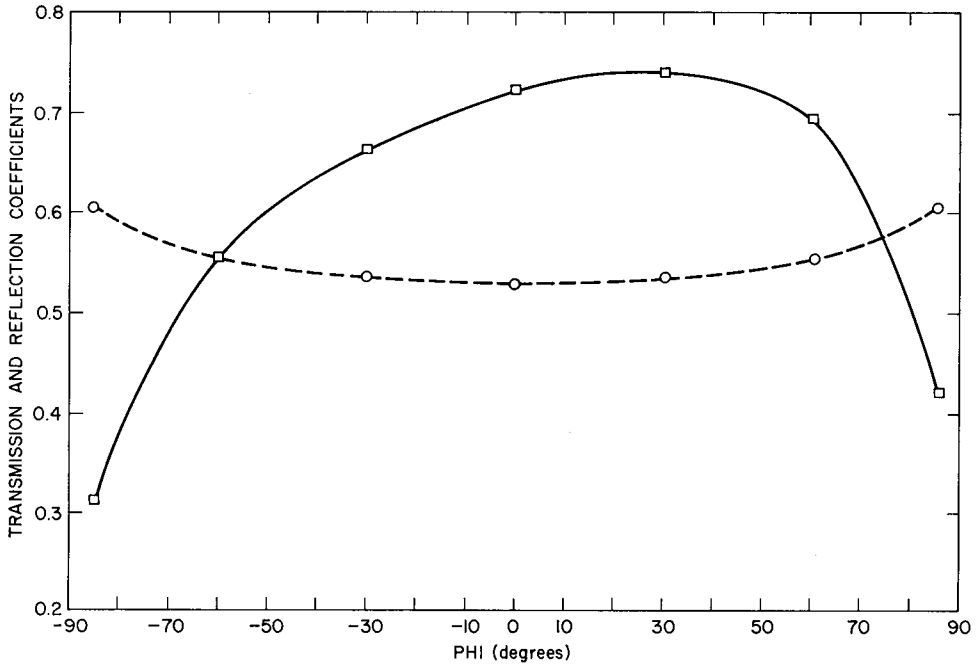


Fig. 5 — Transmission coefficient (solid line) and reflection coefficient (dashed line) vs the angle of incidence from the vertical (PHI) for 3 kHz, dip angle = 60° , and azimuth = 0° (measured from magnetic north)

Figure 7 shows the typical behavior of the hop-dependent part of the TRP factor (the term in braces in Eq. (23)). Note that this term also contains a $\cos^2 \vartheta_a$ dependence. Each curve represents a 3-kHz wave launched in a different direction from the same location (altitude 818.1 km, geomagnetic latitude 43.6556° , geomagnetic longitude 0.0°). Figure 8 shows the geometry determining the initial propagation direction \hat{k} in a local right-hand coordinate system with unit vectors \hat{r} , $\hat{\vartheta}$, $\hat{\phi}$ positive in the directions of increasing altitude, colatitude, and east longitude respectively. The angle δ_ϑ is the angle between \hat{r} and the projection of \hat{k} onto the $r\theta$ plane, and δ_ϕ is the angle between \hat{r} and the projection of \hat{k} onto the $r\phi$ plane. Thus the three cases in Fig. 7 have the following orientation:

Case	δ_ϑ (deg)	δ_ϕ (deg)
a	197.6654	182.4000
b	197.6654	182.6000
c	197.6654	182.6400

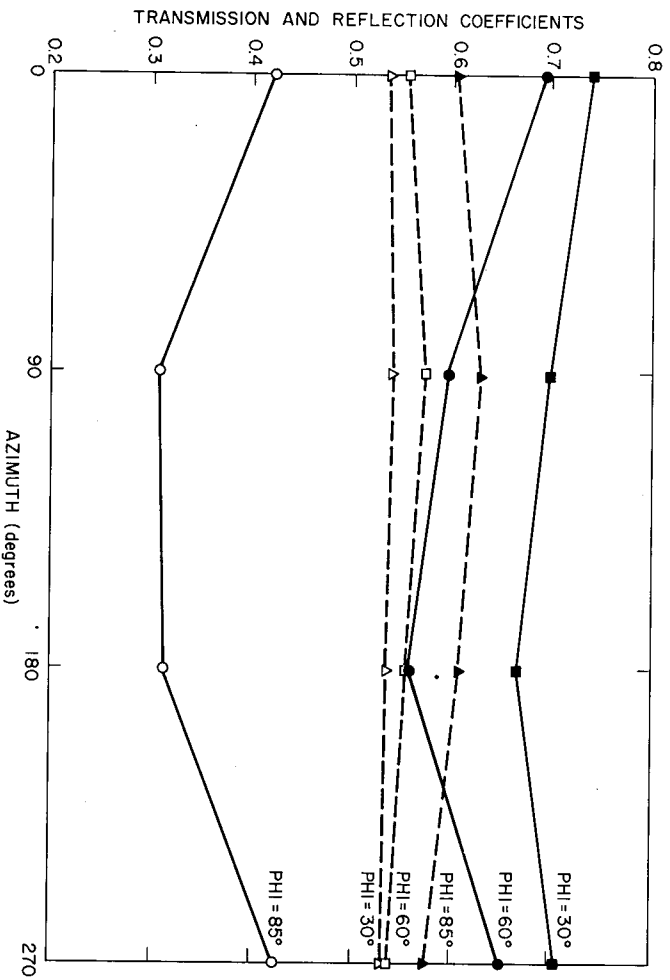


Fig. 6 — Transmission coefficients (solid lines) and reflection coefficients (dashed lines) vs azimuth (measured from magnetic north) for 3 kHz, dip angle = 60°, and angle of incidence from vertical (PHI) = 30°, 60°, and 85°.

Table 2
Transmission and Reflection Coefficients
as a Function of PHI

Fre- quency (kHz)	Dip Angle (Deg)	PHI (Deg)	AZ (Deg)	Bottom Height (km)	Number of Step Sizes per Wavelength	Top Height (km)	Reflec- tion Coeffi- cient	Trans- mission Coeffi- cient
3	60	-85	0	67.5	100	120	0.606	0.313
3	60	-60	0	67.5	100	120	0.555	0.550
3	60	-30	0	67.5	100	120	0.536	0.663
3	60	0	0	67.5	100	120	0.527	0.723
3	60	30	0	67.5	100	120	0.534	0.738
3	60	60	0	67.5	100	120	0.552	0.693
3	60	85	0	67.5	100	120	0.602	0.419

Table 3
Transmission and Reflection Coefficients
as a Function of AZ

Fre- quency (kHz)	Dip Angle (Deg)	PHI (Deg)	AZ (Deg)	Bottom Height (km)	Number of Step Sizes per Wavelength	Top Height (km)	Reflec- tion Coeffi- cient	Trans- mission Coeffi- cient
3	60	85	0	67.50	50	120	0.653	0.400
3	60	85	90	67.50	100	120	0.628	0.306
3	60	85	90	67.50	50	120	0.632	0.375
3	60	85	270	67.50	50	120	0.579	0.524
3	60	60	90	67.50	100	120	0.573	0.596
3	60	60	90	67.50	50	120	0.574	0.734
3	60	60	270	67.50	50	120	0.536	0.803
3	60	30	90	67.50	100	120	0.540	0.698
3	60	30	90	67.50	50	120	0.538	0.862
3	60	30	270	67.50	50	120	0.528	0.870

Table 4
Transmission and Reflection Coefficients
for Various PHI and AZ

Fre- quency (kHz)	Dip Angle (Deg)	PHI (Deg)	AZ (Deg)	Bottom Height (km)	Number of Step Sizes per Wavelength	Top Height (km)	Reflec- tion Coeffi- cient	Trans- mission Coeffi- cient
3	60	85	90	67.50	1000	120	0.622	0.306
3	60	85	90	67.50	100	120	0.628	0.306
3	60	85	180	67.50	100	120	0.606	0.313
3	60	85	270	67.50	100	120	0.575	0.427
3	60	60	90	67.50	100	120	0.573	0.596
3	60	60	270	67.50	100	120	0.539	0.650
3	60	30	90	67.50	100	120	0.540	0.698
3	60	30	270	67.50	100	120	0.532	0.703

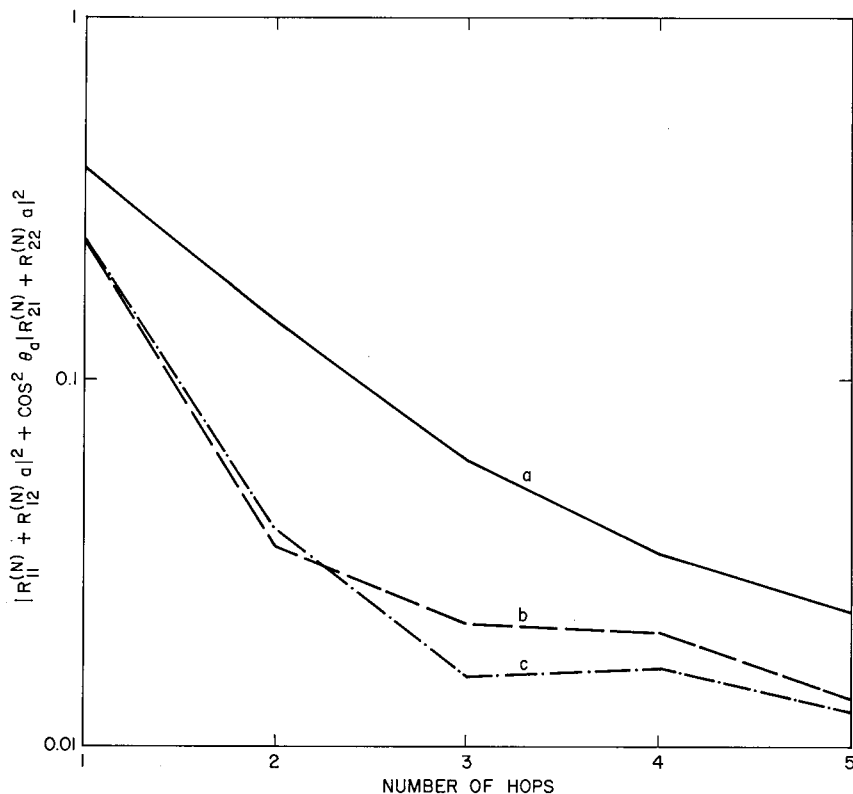


Fig. 7 — Variation of a term in the TRP factor as a function of the number of hops N for three cases

Using Eq. (31), the wave polarization in each case can be calculated as a function of the number of hops. These equations were evaluated for the three cases of Fig. 7, and the results are shown in Fig. 9. Using the convention that if $a = \alpha + i\beta$, with

- | | | |
|--|---|--|
| $\beta = 0 \rightarrow$ | phase = 0, $\pi \rightarrow$ | linear polarization |
| $\alpha \geq 0, \beta > 0 \rightarrow$ | $0 < \text{phase} \leq \pi/2 \rightarrow$ | right elliptic polarization
(negative helicity) |
| $\alpha \leq 0, \beta > 0 \rightarrow$ | $\pi/2 \leq \text{phase} < \pi \rightarrow$ | right elliptic polarization |
| $\alpha = 0, \beta = 1 \rightarrow$ | phase = $\pi/2 \rightarrow$ | right circular polarization |
| $\alpha \leq 0, \beta < 0 \rightarrow$ | $\pi < \text{phase} \leq 3\pi/2 \rightarrow$ | left elliptic polarization
(positive helicity) |
| $\alpha \geq 0, \beta < 0 \rightarrow$ | $3\pi/2 \leq \text{phase} < 2\pi \rightarrow$ | left elliptic polarization |
| $\alpha = 0, \beta = -1 \rightarrow$ | phase = $3\pi/2 \rightarrow$ | left circular polarization |

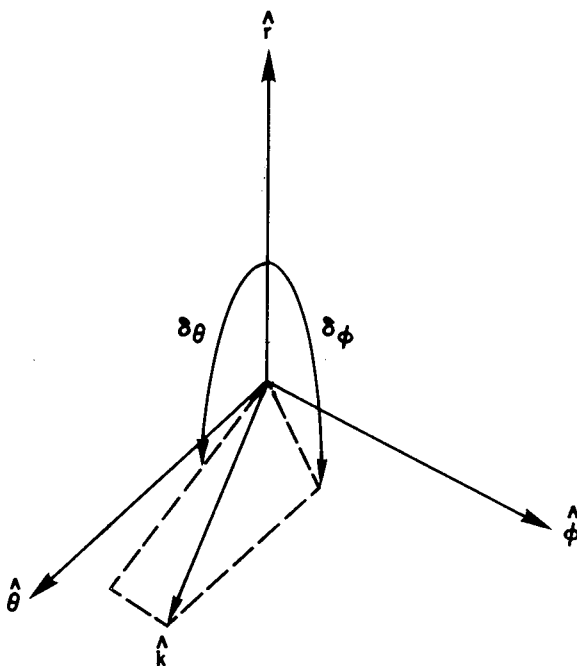


Fig. 8 — Geometry determining the initial propagation direction \hat{k} ; \hat{r} is in the direction of increasing height, $\hat{\theta}$ is in the direction of increasing colatitude, and $\hat{\phi}$ is in the direction of increasing east longitude.

it is seen that in each case the wave started out as right elliptically polarized and changed drastically on each hop. However, the limiting polarization was right elliptical and neared the limiting value after seven hops. It should also be pointed out that Case a and Case b satisfied Eq. (32a), whereas Case c satisfied Eq. (32b).

CONCLUSION

Expressions have been derived and programmed which predict the ratio of power penetrating the sea to the power incident above the ionosphere as a function of the number of wave hops between the earth-ionosphere wave guide. The program also calculates the wave polarization as a function of the number of hops and predicts the resulting polarization after a large number of hops. The program allows these results to be studied as a function of the ionospheric model and point of entry of the incident wave on the ionosphere. Thus these results, when added to those described in other reports [14], allow a signal power budget to be calculated for a magnetospheric source radiating in the ELF or VLF range.

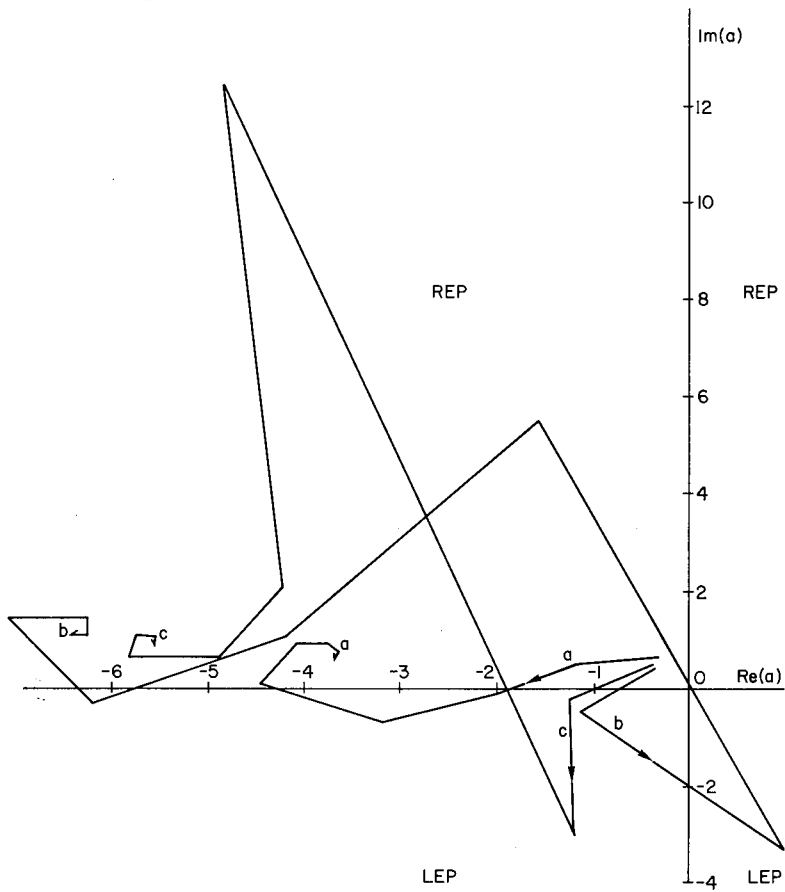


Fig. 9 — Real and imaginary parts of the polarization amplitude a as a function of the number of hops. REP denotes the regions of right elliptical polarization, and LEP denotes the regions of left elliptical polarization.

REFERENCES

1. M.L.V. Pitteway and J.L. Jespersen, *J. Atmos. Terr. Phys.* **28**, 17 (1966).
2. M.L.V. Pitteway, *Phil. Trans. Roy. Soc. A257*, 219 (1965).
3. R.R. Scarabucci, Stamford Electronics Laboratory Technical Report 3412-11 (1969)
4. R.A. Pappert and L.R. Shockey, Naval Electronics Laboratory Center (NELC) Report 722 (1972).
5. R.A. Pappert, R.R. Smith, and L.R. Shockey, NELC Report 712 (1971).
6. R.A. Pappert and R.R. Smith, NELC Report 701 (1970).

7. K.G. Budden, *Radio Waves in the Ionosphere*, Cambridge University Press, 1966; *Proc. Roy. Soc. London* A265, 538 (1962); A227, 516 (1955).
8. J.R. Wait and K.P. Spies, *Radio Sci.* 69D, 1359 (1965).
9. M.B. Kraichman, *Handbook of Electromagnetic Propagation in Conducting Media*, NAVMAT p. 2302, Government Printing Office, 1970.
10. J.R. Wait and K.P. Spies, NBS Technical Note No. 300, Dec. 30, 1964.
[A $\beta = .5 \text{ km}^{-1}$, $h = 70.0 \text{ km}$ daytime ionosphere is used.]
11. J. Galejs, *Terrestrial Propagation of Long Electromagnetic Waves*, Pergamon Press, New York, 1972. [Fig. 7.8 curve C].
12. R.A. Pappert, W.F. Moler, and L.R. Shockley, "A Fortran Program for Waveguide Propagation Which Allows Both Vertical and Horizontal Dipole Excitation," Naval Electronics Laboratory Center Interim Report 702 for DASA, June 1970.
13. G.H. Smith and M.L.V. Pitteway, "Fortran Program for Obtaining Wavefields of Penetrating, Non-penetrating, and Whistler Modes of Radio Waves in the Ionosphere," in *ELF-VLF Radio Wave Propagation* (J. A. Holtet, editor) D. Reidel, Boston 1974.
14. F.J. Kelly, D.J. Baker, and G.A. Chayt, NRL Report 7814, Dec. 31, 1974.